Experimental and numerical exploration of intrinsic localized modes in an atomic lattice

doi: 10.1007/s10867-009-9135-2

Journal of Biological Physics manuscript No.
(will be inserted by the editor)

M. Sato · A. J. Sievers

Experimental and numerical exploration of intrinsic localized modes in an atomic lattice

Received: date / Accepted: date

Abstract This review focuses attention on the experimental studies of intrinsic localized modes (ILMs) produced in driven atomic lattices. Production methods involve the application of the modulational instability under carefully controlled conditions. One experimental approach is to drive the atomic lattice far from equilibrium to produce ILMs, the second is to apply a driver of only modest strength but nearby in frequency to a plane wave mode so that a slow transformation from large amplitude standing waves to ILMs takes place. Since in either case the number of ILMs produced is small the experimental observation tool appropriate for this task is four wave mixing. This nonlinear detection technique makes use of the nonlinearity associated with an ILM to enhance its signal over that produced by the more numerous, but linear, spin waves. The final topic deals with numerical simulations of a nonlinear nanoscale atomic lattice where the new feature is running ILMs.

Keywords Intrinsic localized modes · Discrete breathers · Nonlinear atomic lattices · Modulational instability · Nonlinear mode locking

PACS 05.45.-a · 63.20.Pw · 63.20.Ry

1 Introduction

1.1 Background

The investigation of vibrational energy localization in highly excited small molecules has a long history and a number of reviews have appeared[1–7]. Experiments on molecular overtone and combination bands by means of sensitive absorption, thermal lensing and photoacoustic spectroscopy, particularly involving X-H vibrations, have been interpreted successfully in terms of normal modes for low lying vibrational states and local modes for high lying states. In condensed matter lattices vibrational energy localization can be produced by lattice irregularities and such defect-induced localized modes, which appear above the plane wave spectrum, in the frequency gaps between the plane wave branches, or in the acoustic spectrum, have been studied in great detail both theoretically[8–12] and experimentally[13–15]. For nonlinear atomic lattices the study of localized vibrational energy has a much shorter history. Initially, the continuum approximation and perturbation theory were used to demonstrate that anharmonicity in a 1-D lattice could produce soliton-like excitations, extending over a large number of sites[16]. In the late 1980 ’s it was proposed that the localization of vibrational energy produced by nonlinearity in a discrete lattice could appear above the phonon spectrum and extend over a very few lattice sites[17,18]. Later it was demonstrated with realistic two body potentials that such localized

Graduate School of Natural Science and Technology, Kanazawa University
Kanazawa, Ishikawa 920-1192, Japan E-mail: msato@kenroku.kanazawa-u.ac.jp

Laboratory of Atomic and Solid State Physics, Cornell University
Ithaca, NY 14853-2501, USA

excitations should appear in a phonon gap[19,20]. Since spectroscopically these strongly localized excitations would resemble a feature associated with a harmonic force constant lattice defect they were called intrinsic localized modes (ILMs). They are also referred to as lattice solitons[21] or discrete breathers[22].

1.2 Experimental approaches for identifying ILMs

For a 3-D dielectric diatomic crystal involving two body potentials simulations have shown that an ILM not only involves dynamical localization of vibrational energy but also carries an associated localized dc strain field[23]; hence, its spatial structure in the perfect crystal is similar to that of an intrinsic vibrationally-induced defect. Such a vibrational defect requires more energy to form than does a plane wave excitation but the induced crystal disorder makes it appearance possible since associated with these defects is an additional configurational entropy, S_c [18]. For such a localized crystal defect the Helmholtz free energy is

$$F = F_0 + n\epsilon - TS_c \tag{1}$$

where F_0 is the contribution from the perfect lattice, $n\epsilon$ is the work done in creating n such ILM defects, and $-TS_c$ is the contribution associated with the disorder. Minimization of the free energy with respect to the number of defects n for the limit where the defect number, n, is much smaller than the lattice site number, N , gives

$$n \approx N \exp\left(-\varepsilon/k_B T\right) \tag{2}$$

At elevated temperatures the appearance of such ILMs would contribute an Einstein oscillator-like component to the Debye plane-wave specific heat of a dielectric diatomic solid. Since the specific heat contribution from plane wave optic modes themselves is usually approximated by Einstein oscillators, separating these two different contribution would clearly be challenging; hence, the temperature dependence of the specific heat has not been the unique experimental probe for identifying ILMs in bulk solids.

Spectroscopic measurements on solids provide another way to search for an ILM feature. Evidence of ILMs have been reported in the analysis of resonant Raman spectra in the charge transfer solid PtCls[24]; in the monatomic bcc crystal of ^{4}He where inelastic neutron scattering shows an anomalous optic-like mode[25]; in single crystal alpha-uranium where a localized mode has been identified in the optic branch[26]; in proteins where pico-second pump-probe measurements of the amide I band indicate a self-trapped vibrational state[27,28]; and hydrogen bonded acetanilide where spectral anomalies are interpreted as a signature of vibrational self trapping[29,30]. Each of these examples illustrates the fundamental experimental challenge of exploring ILMs in atomic solids; direct observation of spatial energy localization is not yet possible and the observation of transitions, spectroscopic frequency shifts, or relaxation times of spectral elements are connected to localization by theoretical and numerical analysis.

On the other hand, the combination of a spectroscopic measurement with a cw driver provides a steady state approach with which to examine both the appearance and disappearance of atomic nonlinear localization[31–33]. One experimental approach is to drive the atomic lattice far from equilibrium to produce ILMs but then isolate them by continued steady state driving so they can be studied in detail. A second method is to apply a driver of only modest strength but nearby in frequency to a plane wave mode so that a slow transformation from large amplitude plane waves to ILMs takes place. This second procedure was first tested with macroscopic micromechanical arrays[34]. Both of these kinds of experiments deal with the production and spectroscopic detection of steady state atomic ILMs, the main focus of this review. In the next section the ILM production and approaches for steady state driving methods are outlined. Section 3 deals with the experimental observations of such localized spin excitations in a 1-D antiferromagnetic lattice. This study of large systems is followed in Section 4 by numerical simulations describing what to expect for small nano-scale systems. Conclusions follow in Section 5.

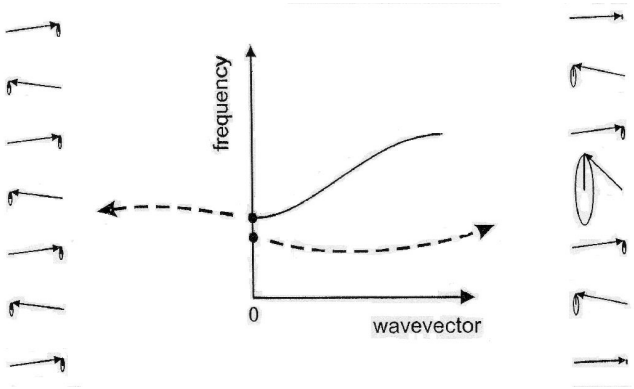

Fig. 1 Delocalized and localized excitations for a 1-D antiferromagnetic arrangement of spins with easy axis anisotropy. The left panel shows the circularly polarized uniform mode eigenvector, the center panel, the linear dispersion curve and the right panel, a localized spin wave excitation.

2 ILM production methods with a cw driver

2.1 Dynamics of an antiferromagnetic spin system

Fundamental to the steady state approach of ILM production in atomic lattice is the modulational instability (MI) of a particular plane wave vibrational mode. MI refers to the exponential growth of certain modulation sidebands of nonlinear plane waves propagating in a dispersive medium[35]. Although many aspects of MI in discrete systems are the same as those in continuous media, the discreteness can drastically alter the modulational instability parameter space[36]. In magnetism the modulational instability of interest for a large amplitude spin wave mode is referred to as the second order Suhl instability[37]. Recent numerical[38–40] and experimental studies[41–46] have shown that antiferromagnets provide a natural habitat for ILMs. Although the dipole active spin wave frequencies of most antiferromagnets are above the frequency range of high power microwave sources a few 1-D antiferromagnets have uniform modes in the GHz region; hence, it is now possible to examine the low lying nonlinear excitations of these atomic systems in the steady state.

The uniform spin wave mode and linear dispersion curve of spin wave excitations for a typical 1-D easy axis uniaxial antiferromagnet, shown in Fig 1, can be obtained by examining the equations of motion. For such a chain, in which each spin interacts with its nearest neighbors via the exchange interaction and each spin feels an on-site anisotropy field, the Hamiltonian is[47]

$$H = 2J \sum_n \mathbf{S}_n \cdot \mathbf{S}_{n+1} - D \sum_n \left(S_n^z\right)^2 \tag{3}$$

where both the exchange constant J and the single ion anisotropy constant D are positive. The classical equations of motion for the circularly polarized spin deviation s_n^+ is

$$ids_n^+/dt = -2J\left[\left(s_{n-1}^z + s_{n+1}^z\right) s_n^+ - \left(s_{n-1}^+ + s_{n+1}^+\right) s_n^z\right] + 2DSs_n^z s_n^+ \tag{4}$$

giving the linear dispersion curve

$$\Omega(q) = \pm\sqrt{(A+2)^2 - 4\cos^2(qa)} \tag{5}$$

Here $\Omega(q) = \omega(q)/2JS$, $A = D/J$, q the wavevector and a is the lattice constant. The antiferromagnetic resonance (AFMR) frequency is $\Omega(0) = \sqrt{A\,(A+4)}$. For the small anisotropy limit the relatively large AFMR frequency associated with the uniform mode is roughly the geometric mean of the exchange and anisotropy fields. A more careful description shows that the sample shape also influences the frequency position of the uniform mode with respect to the rest of the spin wave branch[40]. To obtain the bottom frame in Fig. 1 one assumes a stationary elementary excitation with a circular precession frequency ω_1:

$$s_n^+(t) = s_n(t) \exp\left(-i\omega_\ell t\right) \tag{6}$$

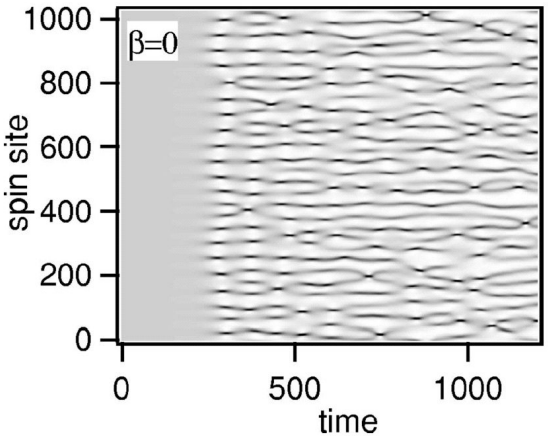

Fig. 2 Evolution of the uniform mode energy density in space versus time. The uniform mode at the bottom of the spin wave band in Fig. 1 is excited at $t = 0$. Dark shading identifies areas of high energy. The large amplitude uniform mode is stable until about 200 periods where it breaks up into ILMs that initially are fairly uniformly spaced. (After Ref. [40].)

Inserting Eq. 6 into Eq. 4 gives a system of nonlinear equations that can support localized solutions, namely,

$$\Omega_\ell s_n = (-1)^n \left\{ \left(\sqrt{1 - s_{n-1}^2} + \sqrt{1 - s_{n+1}^2} \right) s_n + \left[(s_{n-1} + s_{n+1}) + A s_n \right] \sqrt{1 - s_n^2} \right\} \tag{7}$$

where the time variable has been explicitly dropped. With an appropriate symmetry imposed on the mode shape Eq. 7 can be solved numerically for both the ILM frequency and eigenvector. The bottom frame in Fig. 1 illustrates the possible eigenvector shape for a single peaked spin wave ILM. Because of the soft nonlinearity associated with both the exchange and anisotropy energies this large amplitude localized mode appears below the plane wave modes. Once such a localized mode exists in the antiferromagnetic crystal then by introducing a driving cw oscillator producing circularly polarized radiation of sufficient amplitude tuned to frequency ω_ℓ it should be possible to maintain the ILM in a steady state configuration even in the presence of damping.

2.2 Modulational instability of the dipole active mode

The first step along this path then is to produce such ILMs using the modulational instability mechanism. Figure 2 presents a numerical demonstration of what happens to the uniform mode amplitude patterns beyond the Suhl instability for the case when the uniform mode frequency lies on the spinwave dispersion curve. (Other possibilities are described in Ref. [40]). The figure shows the time evolution of the energy at each site in the form of a density plot of spin energy as a function of spin site and time. At $t = 0$ the uniform mode is excited with specific amplitude. After some time interval the uniformity disappears, a fairly regular train of ILMs appears and then disappears as time progresses to be replaced by a random regime.

The power spectrum for the ILM transverse magnetic moment of such a 1-D spin system in the random regime is shown in Fig. 3. Localized excitations appear below the AFMR with a range of frequencies. The conclusion is that driving the modulational instability results in ILMs but at a number of different frequencies; thus, by itself, the MI is not a method of well-defined ILM production. To produce monochromatic ILMs a second ac drive is introduced in addition to the one that produces the modulational instability. Its frequency is necessarily below the linear spin wave spectrum, near the bottom of the distribution of ILM frequencies shown in Fig. 3. If this driver has sufficient strength it can capture ILMs on speaking terms and support them even after the initial MI driver is turned off. The result is monochromatic ILMs in the crystal synchronized to the second steady state driver.

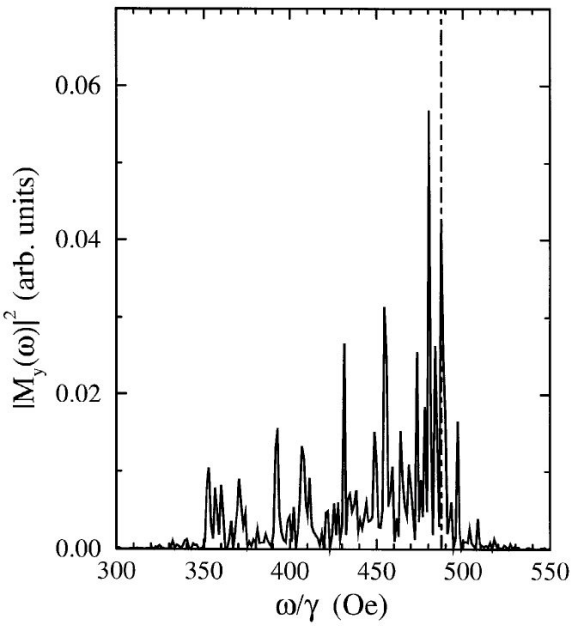

Fig. 3 Power spectrum of the transverse magnetic moments after the modulational instability. A large number of local mode excitations are generated. The dot dashed curve identifies the driving frequency. (After Ref. [39].)

3 Observations of driven ILMs

3.1 Dynamics of the $(C_2H_5NH_3)_2CuCl_4$ spin system

Experiments have been carried out on an easy plane antiferromagnetic crystal, the quasi-1D $(C_2H_5NH_3)_2CuCl_4$. The equation of motion for the normalized spin $\mathbf{S}_n$, including damping and driving terms, is

$$\frac{d}{dt}\mathbf{S}_n = -\gamma \mathbf{S}_n \times \mathbf{H}_n - \gamma\lambda \mathbf{S}_n \times (\mathbf{S}_n \times \mathbf{H}_n) \tag{8}$$

where $vecS_n$ is a macroscopic spin obtained by averaging over the strongly coupled ferromagnetic sheet of spins in the ab plane, γ, the gyromagnetic ratio, and λ, the Landau damping parameter. Here $\mathbf{H}_n$ is the magnetic field acting on the nth macroscopic spin along the c direction where

$$\mathbf{H}_n = -2J\left(\mathbf{S}_{n-1} + \mathbf{S}_{n+1}\right) - 2\overleftrightarrow{A}\mathbf{S}_n + H_{x0}\hat{e}_x \cos\omega t \tag{9}$$

with J, the nearest neighbor antiferromagnetic exchange constant, $\overleftrightarrow{A}$, the anisotropic field tensor, and H_{x0}, the amplitude of the ac driving field along a specific transverse spin direction. For this easy plane case the two dispersion curves (solid circles) are shown in Fig. 4. The branches are no longer degenerate, as in Fig. 1, and are described by an upper branch and a lower branch with the $q = 0$ modes now linearly polarized in orthogonal directions. The experiments described here involved exciting spins at the bottom of the lower branch.

3.2 Pulse method of generating and observing ILMs

Figure 5 illustrates the actual experimental procedure displaying an absorption frequency versus time graph in the neighborhood of the AFMR of the lower branch. A very weak probe oscillator (call it f_3) is swept in frequency to monitor the absorption spectrum. At $t = 0$ the AFMR absorption is located at 1.375 GHz. A strong microwave pulse of short duration (f_1) produces an MI in the spin wave spectrum. A steady state oscillator (f_2) with 1000 times less power is used to capture some ILMs which are passing by this frequency as the spins recovers from the initial high intensity pulse. Notice

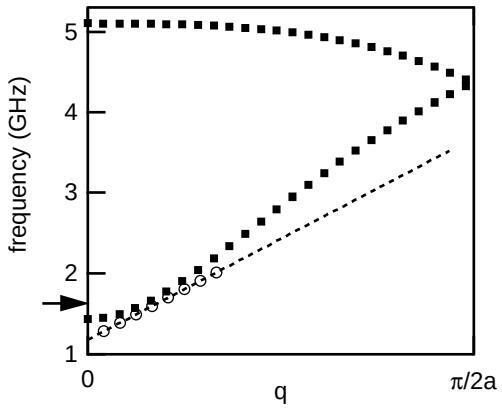

Fig. 4 Dispersion curve of $C_2H_5NH_3)_2CuCl_4$ showing a traveling ILM mode. For $N = 100$ the linear modes are indicated by solid circles. The stationary ILMs that appear below the bottom of the acoustic branch do not depend on sample size. Open circles on the dashed tangent to the dispersion are Fourier components of a traveling ILM for the small system described in Section 4. The ILM velocity coincides with the slope. Because of the finite crystal boundary conditions the excitation of linear modes in the acoustic spectrum and hence runnimng ILMs is possible.

that it takes many milliseconds for the AFMR to return to the starting condition so the frequency gap between f_2 and the AFMR increases with increasing time. Since no absorption feature is evident at frequency f_2 in Fig. 5 the question is how can one determine that ILMs are actually trapped there? The technique is four wave mixing involving the two remaining oscillators f_2 and f_3. Since ILMs are nonlinear by nature while the plane wave modes are essentially linear the mixing technique lights up the few nonlinear excitations and only a much weaker signal stems from the many linear ones.

The ILM sensitivity produced by the four wave mixing method can be seen in Fig. 6 where the emission $(2f_2 - f_3)$ is compared to the linear spin wave absorption spectrum taken with f_3 for 2 ms after the f_1 pulse. The absorption spectrum (linear scale) is quite simple while the more sensitive emission spectrum (log scale) is much richer. The strongest emission peak observed slightly below the f_2 driver is from the monochromatic ILMs. Rather than look at the emission spectrum at fixed time after the f_1 pulse another kind of measurement is to place f_2 on the ILM emission peak and measure its amplitude as a function of time. A family of time dependent traces can be obtained by then varying the power settings of f_2. Such traces are shown in Fig. 7(a) where the square root of the emission power is plotted versus time. Figure 7(b) shows how the individual emission curves can be decomposed into an exponential decay plus steps of equal height demonstrating that individual ILMs are disappearing as the frequency difference between f_2 and the AFMR increases with time. The dotted curve in Fig. 7(b) is the same as the dotted curve in 7(a).

These experiments show that the emitted $P^{(3)}_{ILM}$ power received at the spectrum analyzer is a function of the integer number of locked ILMs, n_{ILM} , that involve magnetization changes of equal increments. The four wave mixing signal has the form[45]

$$\sqrt{P^{(3)}_{ILM}} = n_{ILM}\,(2f_2 - f_3)\,\chi\,(2f_2 - f_3)\,P_2P_3 \tag{10}$$

where $\chi\,(2f_2 - f_3)$ is an effective nonlinear susceptibility, and the powers delivered to the sample by f_2 and f_3 are P_2 and P_3, respectively.

3.3 CW method of generating and observing ILMs

Another experimental method has been uncovered by which ILMs can be made to appear and disappear. With this approach the spin system is not driven far from equilibrium with a high power pulse, instead f_2 is brought sufficiently close to the AFMR so that it alone can produce and capture ILMs[46]. The mechanism is demonstrated by the absorption spectra shown in Fig. 8. In Fig. 8(a) after

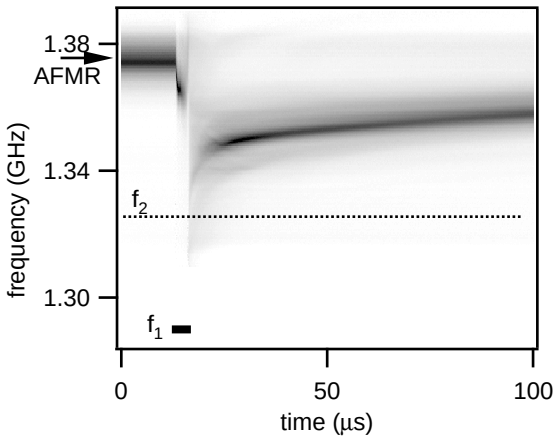

Fig. 5 Absorption spectrum of an antiferromagnetic resonance versus time. The arrow identifies the resonance position at $t = 0$. A strong microwave pulse at frequency f_1 is used to break up the uniform mode. The power of the cw driver f_2 is 1000 times weaker than that of the pulse. (After ref. [45].)

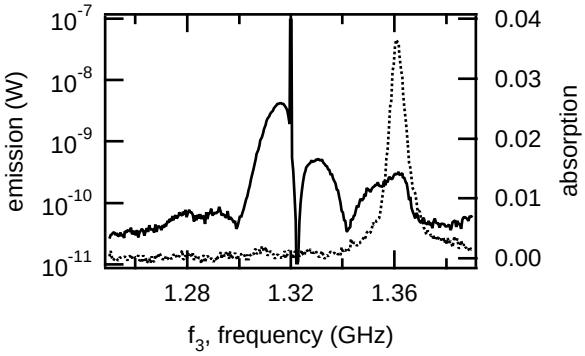

Fig. 6 Snapshot of the emission and absorption spectra 2ms after the f_1 pulse. The small number of ILMs captured by f_2 and seen in the four-wave emission signal is not apparent in the absorption spectrum (dashed trace). In emission the strongest and second strongest peaks on either side of the driver are associated with locked ILMs. (After ref. [45].)

f_2 is turned on at 1.325 GHz the AFMR at 1.38 GHz is pulled to lower frequencies over a time scale of many ms by its coupling to this power source. For Fig. 8(b) f_2 is bought somewhat closer to the AFMR and the process repeated. Now the AFMR frequency is pulled down more rapidly over about 2 ms but then reaches a near plateau where the coupling appears steady. With f_2 still closer, shown in Fig. 8(c), the result is completely different in that the AFMR quickly becomes unstable as indicated by the increase in the line width. When the time dependence of this configuration is examined with four wave mixing ILMs steps are again observed as shown in Fig. 9. Now the ILMs appear as time progresses. The family of curves is generated using different f_2 power levels. These results demonstrate that ILMs are trapped at the f_2 driver frequency. If the f_2 power is increased, more ILMs are trapped; if the power is decreased, fewer ILMs are trapped. Using this method it is possible to follow an ILM through a switching cycle and display the important signature of step hysteresis.

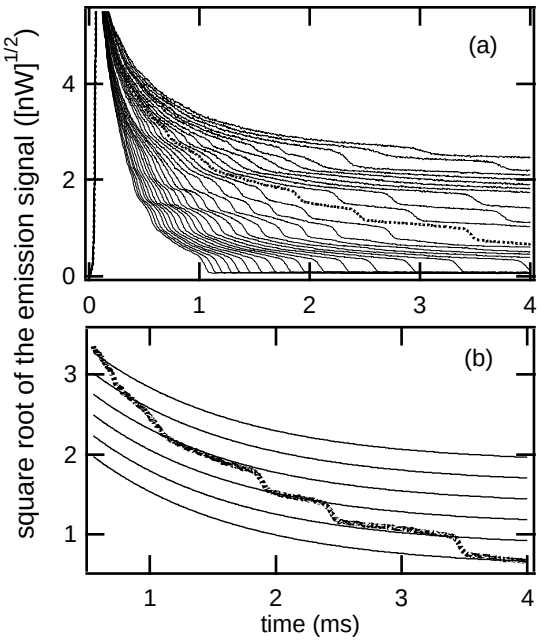

Fig. 7 (a) Square root of the emission decay output versus time for a fixed driving frequency as a function of its cw power. The steps stem from ILMs that become unbound from the driver with increasing time. (b) Characterization of the time dependence of the four-wave emission signal for one of the powers in (a) identified by the dashed curve. The steps are superimposed on an exponential time-dependent background.

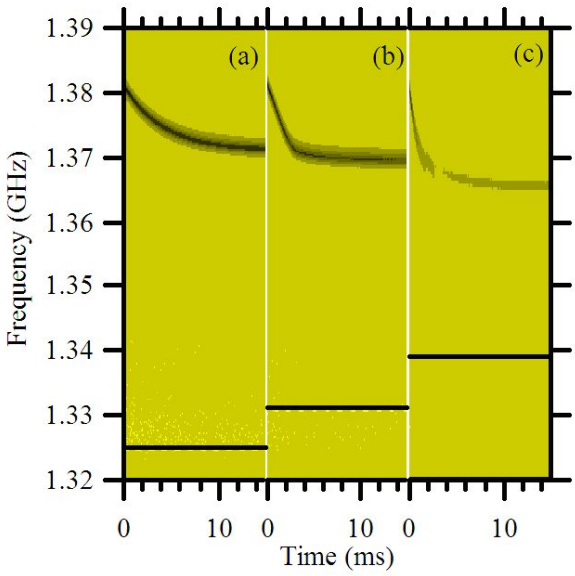

Fig. 8 Pulling the AFMR frequency with a cw driver. (a) The driver at 1.325 GHz is switched on at $t = 0$. It is sufficiently far removed in frequency that the AFMR frequency initially at 1.38 GHz continuously changes over a 15 ms time interval. (b) The gap between the AFMR frequency and the cw driver is small enough so that the change in the AFMR frequency now occurs over 3 ms. (c) The cw driving frequency is sufficiently close to the AFMR mode that it becomes unstable. (After Ref. [46].)

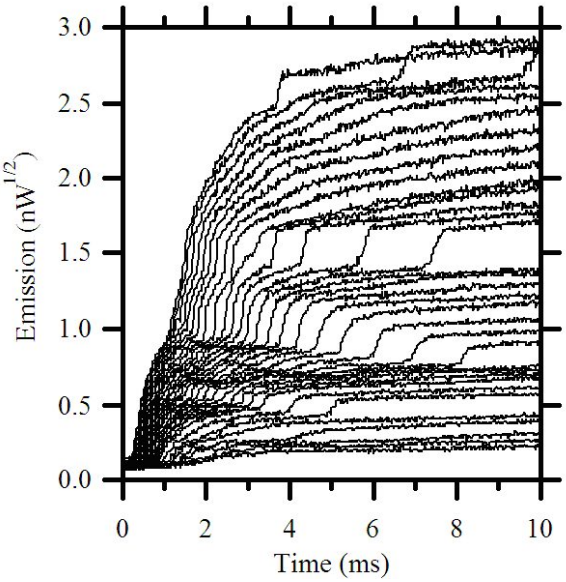

Fig. 9 Square root of the emission growth output versus time for a fixed driving frequency as a function of its cw power. The power is varied from 0.5W to 2W. The cw driver is switched on at $t = 0$ as shown in Fig. 8(c). Positive steps in the emission indicate that ILMs are becoming trapped at the driving frequency. Increasing the cw power produces an increased number of trapped ILMs.

4 Numerical studies of running ILMs in a small atomic lattice

4.1 Modulational instability method for running ILMs

So far the focus of this review has been on experimental studies of atomic ILMs in large lattices. Numerical studies on small nonlinear spin lattices indicate that additional interesting features may be associated with the discrete localization limit[48,49]. In addition to ILMs that appear in the gapped region of the plane wave spectrum of a large lattice, running ILMs can now appear inside the plane wave spectrum of a small lattice. To identify the frequency region of interest attention is again focused on the bottom branch of the linear spin wave dispersion curves of $C_2H_5NH_3)_2CuCl_4$ shown in Fig. 4. Although the highest and lowest frequency modes at $q = 0$ couple most strongly to the E&M driver, for a small system with free boundary conditions, a large number of modes in the spectrum become magnetic dipole active so a single mode of odd symmetry (wavelength $\lambda = 2L/n$, where L is the sample length and n is an odd number) can be excited by simply adjusting the uniform driver to its frequency. The arrow in Fig. 4 identifies a typical driver frequency location near the bottom of the dispersion curve between two standing plane wave modes in the frequency region where soft (negative) nonlinearity can balance positive dispersion. In this dispersion curve picture the signature of the localized wave packet has a spread in values along the q-axis, the more spatially localized the excitation the larger its spread in q-space. The open circles in the figure represent the FT of the ILM. In the simulations described below the polarization of the driving E&M wave for the lower branch frequencies is chosen to match that of the upper branch to suppress exciting the strong low frequency AFMR.

To generate a traveling ILM the driving frequency is chosen near an appropriate linear mode. (This will become the carrier frequency of the traveling ILM.) Because of the small size of the system a well-defined frequency gap exists between that mode and the next higher frequency one. Figure 10 shows the average energy for the lattice excitation as a function of driving frequency between two lattice modes. As the driving frequency is decreased across the first mode at 1.8297 GHz the mode keeps resonating with the driver by adjusting its resonance frequency so that the decreasing frequency supports increasing amplitude. The MI induces the complex running mode pattern shown in insert (a); then at lower frequencies the locked running ILM state in inset (b) appears. This localized feature is one side of a bi-stable state, the other side is a no-mode state, characteristic of the hysteresis response of a Duffing oscillator[50]. The sequence of events to obtain a traveling ILM then is (1) identify a plane

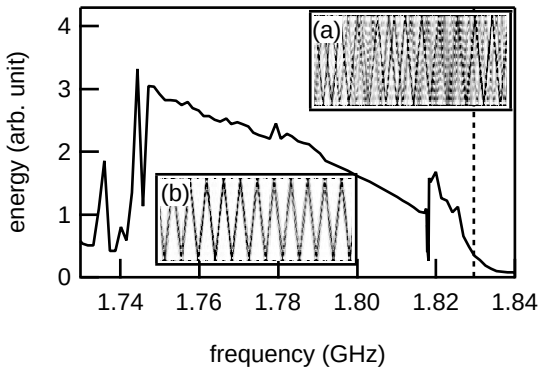

Fig. 10 Calculated energy of spins averaged over the lattice as a function of driver frequency for $N = 100$. Vertical dashed line (1.8297 GHz) identifies the frequency of a linear mode; the next linear mode is at 1.74 GHz. Insert (a) shows spin number versus time. The complex traveling mode pattern shown occurs in the frequency region between 1.8183 to 1.826 GHz. The smooth traveling ILM (insert b) is observed for frequencies between 1.747 to 1.8176 GHz. Both patterns are generated from the MI of the plane wave mode at 1.8297 GHz. The frequencies of inserts (a) and (b) are 1.8183 Hz and 1.8176 GHz, respectively. The time interval for each insert is 180 ns. Spikes at 1.736, 1.7402, 1.7444 and 1.7794 GHz occur at instabilities within the averaging 3000 period time duration.

wave mode in the region where the nonlinearity balances the dispersion, (2) slowly decrease the driver frequency so the plane wave nonlinear mode grows in amplitude reaching the modulational instability, (3) decrease the driver frequency farther until a single traveling ILM is resolved. When the driver frequency is decreased from either the ILM or the no-ILM high frequency state, the system always goes back into the unstable region. Only by decreasing the driver frequency does the system have the opportunity to reach the traveling ILM state.

4.2 Nanoscale size limitations

Numerical simulation results of traveling ILMs for spin arrays in three different size lattices are shown in Fig. 11. The horizontal lines indicate the plane wave mode frequencies. The open circles identify frequencies where locked smoothly traveling ILMs are found. Crosses correspond to frequency regions of instability involving complex traveling modes. The complexity comes about when some overtone of the ILM frequency couples to the linear phonon band. In general smoothly traveling ILMs appear at frequencies below these unstable regions. As the linear modes become closely spaced with increasing system size, in addition to the overtone frequencies of the ILM coupling to the plane wave modes, the driven ILM from the Nth carrier mode interacts with the driven complex mode of the $N + 1$st mode and becomes unstable. The end result is that large systems cannot have discrete stable running ILMs.

The small size limitation for running ILMs in a nanoscale system, which is beginning to show itself for $N = 50$ in Fig. 11, comes about when the spatial extent of the ILM becomes a recognizable fraction of the sample size itself. Because the frequency, size and amplitude of an ILM are interrelated and because its frequency shift from one plane wave mode is bounded by the neighboring plane wave mode frequency, the range of the driven ILM amplitude is limited. This restricted amplitude sets a lower bound on the spatial extent of such a running mode.

5 Conclusions

Experimental studies of a 1-D antiferromagnetically coupled spin systems provide insights into atomic ILMs. Since both onsite and intersite nonlinearity play a role the results can be somewhat different from those expected for vibrational modes in an atomic lattice where only intersite nonlinearity is important. For an antiferromagnet with easy uniaxis anisotropy the acoustic-like spin wave modes are degenerate and are gapped both below and above the plane wave spectrum. Since both exchange

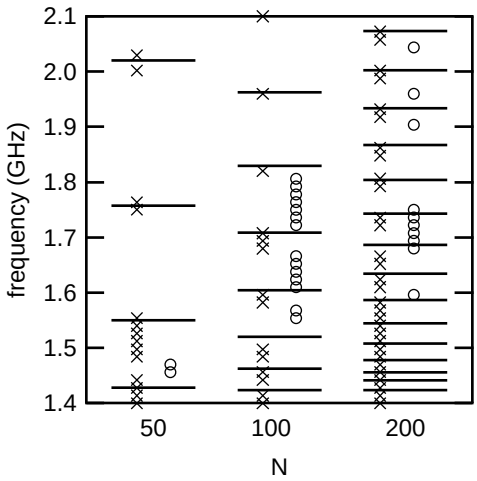

Fig. 11 Numerical simulation results for the dependence of traveling locked ILMs on system size. Horizontal lines identify spin wave modes of the lower branch that can be excited by the ac field polarized along the upper branch $q = 0$ direction due to the finite lattice size with free boundary conditions. Crosses indicate frequencies for the complex traveling modes and open circles identify smoothly traveling mode locations. The frequency of the smoothly running mode is always lower than the complex mode, when they stem from the same carrier mode. (After Ref. [49].)

and anisotropy nonlinearity are soft ILMs can drop out of the bottom of the plane wave spectrum. For the antiferromagnet with hard uniaxis anisotropy (the case studied here in experiment) there are nondegenerate acoustic and optic-like branches. Because of the soft nonlinearity and the fact that the two branches are degenerate at the zone boundary ILMs only drop out of the bottom of the plane wave acoustic branch. Numerical simulations show that for such a spin system of small size running ILMs can be excited within the plane wave spectrum.

There have been a variety of experiments carried out on macroscopic nonlinear lattices, not discussed here, where visual inspection can be used to identify localization[51,52]. These range from electric transmission lines[53–56], to electromagnetic waves in nonlinear layered structures[57,58], to coupled pendula[59–61], to arrays of Josephson junctions[62,63], to 2-D photonic crystal lattices[64, 65], to micromechanical arrays[66]. The ILM observations obtained for the 1-D spin system described here complement rather nicely the ILMs measured for micromechanical arrays[34]. Since the array has two cantilevers of different length per unit cell the plane wave spectrum contains an acoustic and optic branch with frequency versus k-vector shapes very similar to those found in Fig. 4 for the antiferromagnet. However, for the micromechanical array both the intersite and on site nonlinearity are hard so stationary ILMs now rise out of the top of the optic branch[34]. By driving a small MEMS array it is possible to excite running ILMs, of either the bright (localized excitation present) or dark (localized excitation absent) variety[49].

The experimental results for the 1-D antiferromagnet are expected to be less complex than ILMs involving a 1-D atomic lattice with realistic two body potentials. The main reason is that whereas the spin dynamics involves potential energy terms of even powers the two body potentials in lattice dynamics involve both even and odd potential terms. The odd potential terms not only insure that the nonlinearity of the lattice is soft but also introduce a new feature: a localized dc distortion at the ILM site. To move this ILM through the lattice requires simultaneous motion of both the localized vibrational energy and the localized dc elastic distortion energy. Driving a small 1-D lattice would necessarily take more power to generate and sustain this more complex localized structure across the lattice than for the spin problem but locked running ILMs should still be possible. This two body potential form should also allow counterpropagating ILMs in a small lattice by driving it at the ILM harmonic frequency so that localized excitations at q and $-q$ are simultaneously produced.

Additional new ILM features may be expected to occur in a 3-D atomic lattice. For example, if the crystal symmetry is lowered from O_h to T_d the importance of nonlinearity and hence ILMs will more rapidly become evident[23]. If the crystal is piezoelectric then formation of an ILM will consist of a

localized vibration, a localized dc distortion and a localized dc electric dipole moment. Since the ILM dc distortion will have a lower symmetry than the corresponding crystal point group there must be a number of equivalent directions associated with this dc distortion and localized electric dipole moment. One could expect hindered rotation or tunneling to occur between such equivalent configurations at a given lattice location so that on average the point group symmetry of the crystal is recovered.

Acknowledgements This work was supported in part by DOE No. DE-FG02-04ER46154 and by JSPS-Grant-in-Aid for Scientific Research No. (B) 18340086.

References

1. Henry, B. R.: Local modes and their application to the analysis of polyatomic overtone spectra, J. Phys. Chem. 80, 2160-2164 (1976)
2. Henry, B. R.: The use of local modes in the description of highly vibrationally excited molecules, Acc. Chem. Res. 10, 207-213 (1977)
3. Henry, B. R.: The local mode model. In: Durig, J. R., (ed.) Vibrational Spectra and Structure, vol. 10, pp. 269-319. Elsevier, New York, (1981)
4. Sage, M. L. and Jortner, J.: Bond modes, Adv. Chem. Phys. 47, 293-323 (1981)
5. Child, M. S. and Halonen, L.: Overtone frequencies and intensities in the local mode picture, Adv. Chem. Phys. 57, 1-57 (1984)
6. Henry, B. R.: The local mode model and overtone spectra: A probe of molecular structure and conformation, Acc. Chem. Res. 20, 429-435 (1987)
7. Henry, B. R. and Kjaergaard, H. G.: Local modes, Can. J. Chem. 80, 1635-1642 (2002)
8. Lifshitz, I. M.: Some problems of the dynamic theory of non-ideal crystal lattices, Nuovo Cim. Suppl. 3, 716-734 (1956)
9. Maradudin, A. A., Montroll, E. W. and Weiss, G. H.: Theory of Lattice Dynamics in the Harmonic Approximation. In Seitz, F. Turnbull, D., (eds.) Solid State Physics Supplement 3, Academic Press, New York, (1963)
10. Lifshitz, I. M. and Kosevich, A. M.: The dynamics of a crystal lattice with defects, Rep. Prog. Phys. 29, 217-254 (1966)
11. Maradudin, A. A., Montroll, E. W., Weiss, G. H. and Ipatova, I. P.: Theory of Lattice Dynamics in the Harmonic Approximation. Academic Press New York (1971), vol. 3
12. Bilz, H., Strauch, D. and Wehner, R. K.: Vibrational Infrared and Raman Spectra of Non-Metals. Genzel, L., (ed.) Handbuch der Physik vol. XXV, Pt. 2d, Springer-Verlag Berlin, (1984),
13. Sievers, A. J.: Localized and resonance states in ionic crystals. in: Wallis, R. F., (ed.) Localized Excitations in Solids, pp. 27-45. Plenum Press, New York, (1968)
14. Newman, R. C.: Infra-red absorption due to localized modes of vibration of impurity complexes in ionic and semiconducting crystals. Adv. Phys. 18, 545-663 (1969)
15. Barker, A. S. and Sievers, A. J.: Optical studies of the vibrational properties of disordered solids. Rev. Mod. Phys. 47, S1-S179 (1975)
16. Kosevich, A. M. and Kovalev, A. S.: Self-localization of vibrations in a one-dimensional anharmonic chain, Sov. Phys.-JETP 40, 891-896 (1974)
17. Dolgov, A. S.: The localization of vibrations in a nonlinear crystal structure. Sov. Phys. Solid State 28, 907-910 (1986)
18. Sievers, A. J. and Takeno, S.: Intrinsic localized modes in anharmonic crystals. Phys. Rev. Lett. 61, 970-973 (1988)
19. Kiselev, S. A., Bickham, S. R. and Sievers, A. J.: Anharmonic gap modes in a perfect 1-D diatomic lattice for standard two-body nearest-neighbor potentials. Phys. Rev. B 48, 13508-13511 (1993)
20. Sievers, A. J. and Page, J. B.: Unusual Anharmonic Local Mode Systems. In: Norton, G. K. Maradudin, A. A., (eds.) Dynamical Properties of Solids: Phonon Physics The Cutting Edge, vol. VII, pp. 137-255. North Holland, Amsterdam, (1995)
21. Christodoulides, D. N. and Joseph, R. I.: Discrete self-focusing in nonlinear arrays of coupled waveguides. Opt. Lett. 13, 794-796 (1988)
22. Flach, S. and Willis, C. R.: Discrete breathers. Phys. Repts. 295, 182-264 (1998)
23. Kiselev, S. A. and Sievers, A. J.: Generation of intrinsic vibrational gap modes in three-dimensional ionic crystals. Phys. Rev. B 55, 5755-5758 (1997)
24. Swanson, B. I., Brozik, J. A., Love, S. P., Strouse, G. F., Shreve, A. P., Bishop, A. R., Wang, W.-Z. and Salkola, M. I.: Observation of intrinsically localized modes in a discrete low dimensional material. Phys. Rev. Lett. 82, 3288-3291 (1999)
25. Markovich, T., Polturak, E., Bossy, J. and Farhi, E.: Observation of a new excitation in bcc He-4 by inelastic neutron scattering. Phys. Rev. Lett. 88, 195301 (2002)
26. Manley, M. E., Yethiraj, M., Sinn, H., Volz, H. M., Lashley, J. C., Hults, W. L., Lander, G. H. and Smith, J. L.: Formation of a new dynamical mode in alpha-uranium observed by inelastic x-ray and neutron scattering. Phys. Rev. Lett. 96, 125501 (2006)
27. Xie, A., van der Meer, L., Hoff, W. and Austin, R. H.: Long-lived Amide I vibrational modes in myoglobin. Phys. Rev. Lett. 84, 5435-5438 (2000)

28. Austin, R. H., Xie, A. H., van der Meer, L., Shinn, M. and Neil, G.: Self-trapped states in proteins. J. Phys.: Cond. Matter 15, S1693-S1698 (2003)
29. Edler, E., Hamm, P. and Scott, A. C.: Femtosecond study of self-trapped vibrational excitons in crystalline acetanilide. Phys, Rev. Lett. 88, 067403 (2002)
30. Edler, J. and Hamm, P.: Spectral response of crystalline acetanilide and N-methylacetime: Vibrational sel-trapping in hydrogen-bonded crystals. Phys. Rev. B 69, 214301 (2004)
31. Rossler, T. and Page, J. B.: Intrinsic localized modes in driven anharmonic lattices with realistic potentials. Phys. Lett. A 204, 418-426 (1995)
32. Rossler, T. and Page, J. B.: Driven intrinsic localized modes and their stability in anharmonic lattices with realistic potentials. Physica B 220, 387-389 (1996)
33. Maniadis, P. and Flach, S.: Mechanism of discrete breather excitation in driven micro-mechanical cantilever array. Europhys. Lett. 74, 452-458 (2006)
34. Sato, M., Hubbard, B. E. and Sievers, A. J.: Nonlinear energy localization and its manipulation in micromechanical oscillator arrays. Rev. Mod. Phys. 78, 137-157 (2006)
35. Taniuti, T. and Washimi, H.: Self-trapping and instability of hydromagnetic waves along the magnetic field in a cold plasma. Phys, Rev. Lett. 21, 209-212 (1968)
36. Kivshar, Y. S. and Peyrard, M.: Modulational instabilities in discrete lattices. Phys. Rev. A 46, 3198-3205 (1992)
37. Suhl, H.: The theory of ferromagnetic resonance at high signal powers. J. Phys. Chem. Solids 1, 209-227 (1957)
38. Lai, R. and Sievers, A. J.: Modulational instability of nonlinear spin waves in easy axis antiferromagnetic chains. Phys. Rev. B 57, 3433-3443 (1998)
39. Lai, R. and Sievers, A. J.: Nonlinear nanoscale localization of magnetic excitations in atomic lattices. Phys. Repts. 314, 147-236 (1999)
40. English, L. Q., Sato, M. and Sievers, A. J.: Modulational instability of nonlinear spin waves in easy axis antiferromagnetic chains. II Influence of sample shape on intrinsic localized modes and dynamic spin defects. Phys. Rev. B 67, 024403 (2003)
41. Schwarz, U. T., English, L. Q. and Sievers, A. J.: Experimental generation and observation of intrinsic localized spin wave modes in an antiferromagnet. Phys. Rev. Lett. 83, 223-227 (1999)
42. English, L. Q., Sato, M. and Sievers, A. J.: Nanoscale intrinsic localized modes in an antiferromagnet. J. Appl. Phys. 89, 6707-6709 (2001)
43. Sato, M., English, L. Q., Hubbard, B. E. and Sievers, A. J.: Influence of sample shape on the production of intrinsic localized modes in an antiferromagnetic lattice. J. Appl. Phys. 91, 8676-8678 (2002)
44. Sato, M. and Sievers, A. J.: Direct observation of the discrete character of intrinsic localized modes in an antiferromagnet. Nature 432, 486-488 (2004)
45. Sato, M. and Sievers, A. J.: Counting discrete emission steps from intrinsic localized modes in a quasi-1D antiferromagnetic lattice. Phys. Rev. B 71, 214306 (2005)
46. Wrubel, J. P., Sato, M. and Sievers, A. J.: Controlled switching of intrinsic localized modes in a one-dimensional lattice. Phys. Rev. Lett. 95, 264101 (2005)
47. Lai, R., Kiselev, S. A. and Sievers, A. J.: Intrinsic localized spin-wave modes in antiferromagnetic chains with single-ion easy-axis anisotropy. Phys. Rev. B 54, R12665 (1996)
48. Morgante, A. M., Johansson, M., Aubry, S. and Kopidakis, G.: Breather-phonon resonances in finite-size lattices. J. Phys. A-Math. Gen. 35, 4999-5021 (2002)
49. Sato, M. and Sievers, A. J.: Driven localized excitations in the acoustic spectrum of small nonlinear macroscopic and microscopic lattices. Phys. Rev. Lett. 98, 214101 (2007)
50. Jose, J. V. and Saletan, E. J.: Classical Dynamics: A Contemporary Approach. Cambridge University Press, Cambridge, (1998)
51. Campbell, D. K., Flach, S. and Kivshar, Y. S.: Localizing energy through nonlinearity and discreteness. Physics Today 57, 43-49 (2004)
52. Scott, A. C.: Nonlinear Science: Emergence and Dynamics of Coherent Structures. Oxford University Press, New York, (1999)
53. Scott, A. C.: Active Nonlinear Wave Propagation in Electronics. Wiley-Interscience, New York, (1970)
54. Sato, M., Yasui, S., Hikihara, T. and Sievers, A. J.: Management of localized energy in discrete nonlinear transmission lines. Europhys. Lett. 80, 30002 (2007)
55. Stearrett, R. and English, L. Q.: Experimental generation of intrinsic localized modes in a discrete electrical transmission line. J. Phys. D-Appl. Phys. 40, 5394-5398 (2007)
56. Remoissenet, M.: Waves Called Solitons. Springer-Verlag, Berlin, (1999)
57. Chen, W. and Mills, D. L.: Gap solitons and the nonlinear optical response of superlattices. Phys. Rev. Lett. 58, 160-163 (1987)
58. Mills, D. L.: Nonlinear Optics: Basic Concepts. Springer-Verlag, Berlin, (1991)
59. Chen, W.-Z.: Experimental observation of solitons in a 1-D lattice. Phys. Rev. B 49, 15063 (1994)
60. Lou, S. and Huang, G.: Experimental study of the solitons in nonlinear diatomic macro-lattices. Mod. Phys. Lett. B 9, 1231-1241 (1995)
61. Thakur, R. B., English, L. Q. and Sievers, A. J.: Driven intrinsic localized modes in a coupled pendulum array. J. Phys. D-Appl. Phys. 41, 015503 (2008)
62. Trias, E., Mazo, J. J. and Orlando, T. P.: Discrete breathers in nonlinear lattices: Experimental detection in a Josephson array. Phys. Rev. Lett. 84, 741-744 (2000)
63. Binder, P., Abraimov, D., Ustinov, A. V., Flach, S. and Zolotaryuk, Y.: Observation of breathers in Josephson ladders. Phys. Rev. Lett. 84, 745-748 (2000)

64. Mandelik, D., Eisenberg, H. S., Silberberg, Y., Morandotti, R. and Aitchison, J. S.: Observation of mutually trapped multiband optical breathers in waveguide arrays. Phys. Rev. Lett. 90, 253902 (2003)
65. Fleischer, J. W., Segev, M., Efremidis, N. K. and Christodoulides, D. N.: Observation of two-dimensional discrete solitons in optically induced nonlinear photonic lattices. Nature 422, 147-150 (2003)
66. Sato, M., Hubbard, B. E., Sievers, A. J., Ilic, B., Czaplewski, D. A. and Craighead, H. G.: Observation of locked intrinsic localized vibrational modes in a micromechanical oscillator array. Phys. Rev. Lett. 90, 044102 (2003)